

A Study of Supersonic Turbulence in Stagnating Plasma

E. Stambulchik, E. Kroupp, A. Starobinets,
D. Osin, V. I. Fisher, D. Alumot, and Y. Maron¹
S. Davidovits and N. J. Fisch²
A. Fruchtman³

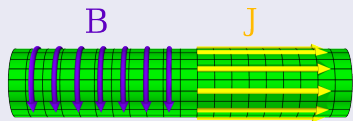
¹Weizmann Institute of Science, Rehovot 7610001, Israel

²Princeton University, Princeton, New Jersey 08540, USA

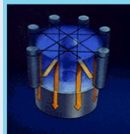
³H.I.T.—Holon Institute of Technology, Holon 5810201, Israel

11th Serbian Conference on Spectral Line Shapes in Astrophysics
Šabac, Serbia
August 21–25, 2017

How Z-pinch works



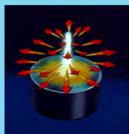
The $\vec{J} \times \vec{B}$ Lorentz force makes the plasma implode.



Initiation



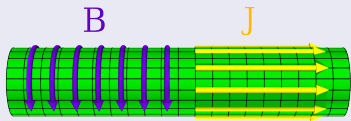
Implosion



Stagnation

Most of the X-ray emission takes place at the stagnation phase.

How Z-pinch works

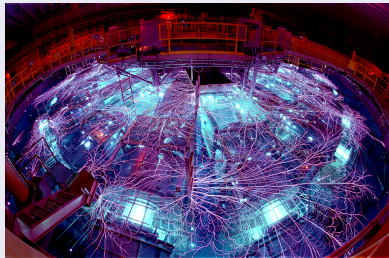


The $\vec{J} \times \vec{B}$ Lorentz force makes the plasma implode.

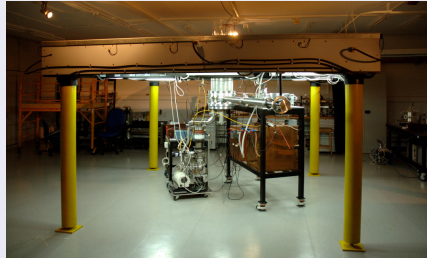


Most of the X-ray emission takes place at the stagnation phase.

“Z machine” (Sandia Labs, US)



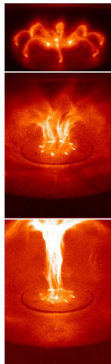
Z-pinch in Weizmann Inst. (Israel)



Focus: Plasma Jets on Earth

August 2, 2005 • Phys. Rev. Focus 16, 4

A simple arrangement of electric and magnetic fields causes plasma to form shapes reminiscent of the jets generated near supermassive black holes.



Phys. Rev. Lett. 95, 095002 (2005)

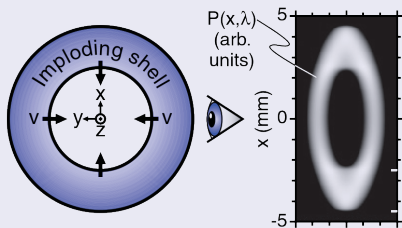
[You et al., 2005]

“A simple arrangement of electric and magnetic fields causes plasma to form shapes reminiscent of the jets generated near supermassive black holes.”

Pinching is a naturally occurring phenomenon, but importance of z-pinches as an astrophysical laboratory goes well beyond that.

Pinches as laboratory astrophysics: im/explosions

Z-pinch ($r \sim 1$ cm)



[Foord et al., 1994]

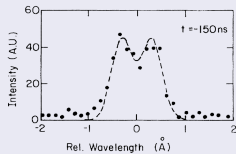
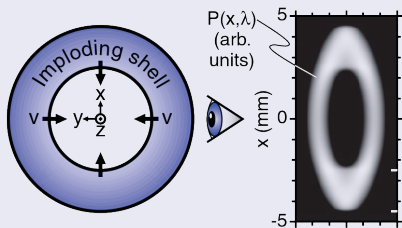


FIG. 2. A typical O III line profile ($\lambda_0 = 3047.1 \text{ \AA}$ measured radially at $z = 11$ mm and $t' = -150$ ns. Redshifted and blueshifted components from each side of the annulus are observed. Doppler shifts correspond to a radial velocity ≈ 3 cm/ μ s.

Pinches as laboratory astrophysics: im/explosions

Z-pinch ($r \sim 1$ cm)



[Foord et al., 1994]

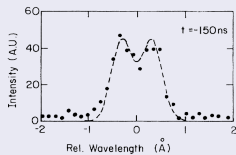
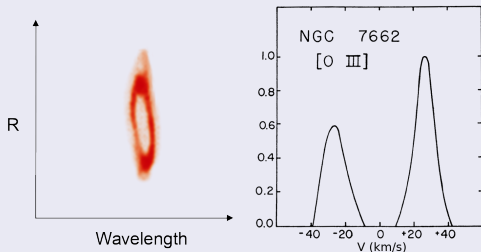


FIG. 2. A typical O III line profile ($\lambda_0 = 3047.1 \text{ \AA}$ measured radially at $z = 11$ mm and $t' = -150$ ns. Redshifted and blueshifted components from each side of the annulus are observed. Doppler shifts correspond to a radial velocity ≈ 3 cm/ μ s.

NGC 7662 ($r \sim 1$ ly)

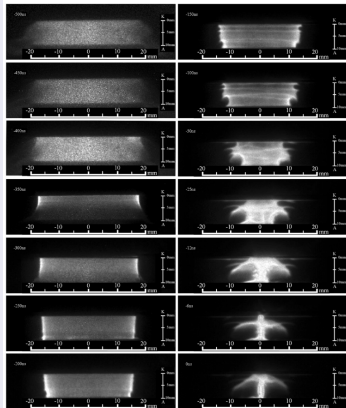


[Osterbrock et al., 1966]



Pinches as laboratory astrophysics: instabilities

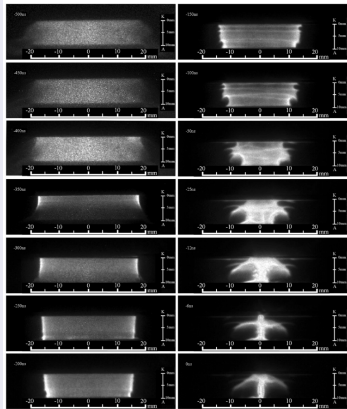
[Osin et al., 2011]



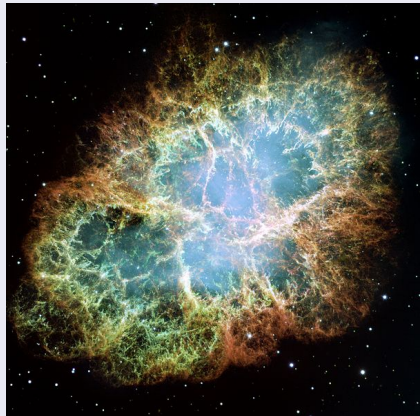
Rayleigh-Taylor instability produces “fingers” and filaments.

Pinches as laboratory astrophysics: instabilities

[Osin et al., 2011]



NGC 1952 (Crab Nebula)

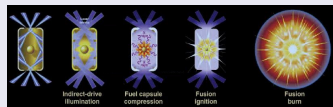


Rayleigh-Taylor instability produces “fingers” and filaments.

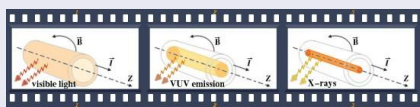
Energy conversion in imploding plasmas

Imploding plasmas are promising candidates for fusion (NIF, MagLIF) and unique sources of intense x-ray radiation (z-pinches).

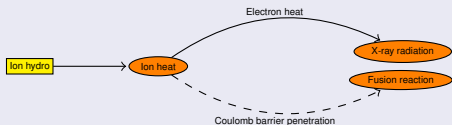
NIF



Z-pinch



Conversion of hydrodynamic ion motion



Thus, one needs to measure ion T_i . It is also important to know the hydro energy.

Principal difficulty:

The Doppler broadening (also, neutron spectrum) gives information only on the **total** ion velocity distribution $\rightarrow T_i^{\text{eff}} \geq T_i$.

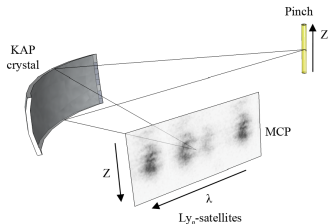
Importance of distinguishing between T_i^{eff} and T_i

Assuming $T_i = T_i^{\text{eff}}$ may result in crucially misinterpreted data.

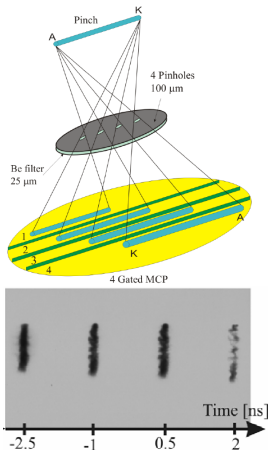
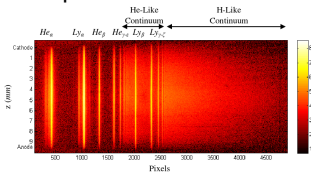
At WIS, we have succeeded developing advanced diagnostics capable of telling T_i^{eff} and T_i apart.

Diagnostics setup

Three time-resolved data sources: spectra of Ne Ly- α dielectronic satellites, gated x-ray pinhole imaging, and an absolutely calibrated photo-conductive detector (PCD) sensitive to $\hbar\omega \gtrsim 700$ eV.



In addition, time-integrated wide spectrum is taken.



Plasma parameters inferred

Assuming the plasma is uniform, we obtain

- Plasma radius r_{pl} – from the pinhole x-ray imaging;

Plasma parameters inferred

Assuming the plasma is uniform, we obtain

- Plasma radius r_{pl} – from the pinhole x-ray imaging;
- Electron density n_e – from the satellite ratios;

Plasma parameters inferred

Assuming the plasma is uniform, we obtain

- Plasma radius r_{pl} – from the pinhole x-ray imaging;
- Electron density n_e – from the satellite ratios;
- Electron temperature T_e – from the time-dependent collisional-radiative (CR) model satisfying both the absolute PCD signal I_{PCD} and time-integrated continuum slope;

Plasma parameters inferred

Assuming the plasma is uniform, we obtain

- Plasma radius r_{pl} – from the pinhole x-ray imaging;
- Electron density n_e – from the satellite ratios;
- Electron temperature T_e – from the time-dependent collisional-radiative (CR) model satisfying both the absolute PCD signal I_{PCD} and time-integrated continuum slope;
- T_i^{eff} – from the satellite Doppler broadening (the Stark width is negligible);

Plasma parameters inferred

Assuming the plasma is uniform, we obtain

- Plasma radius r_{pl} – from the pinhole x-ray imaging;
- Electron density n_e – from the satellite ratios;
- Electron temperature T_e – from the time-dependent collisional-radiative (CR) model satisfying both the absolute PCD signal I_{PCD} and time-integrated continuum slope;
- T_i^{eff} – from the satellite Doppler broadening (the Stark width is negligible);

T_i is inferred from the data above, plus using either

- Detailed energy-balance analysis [Kroupp et al., 2011, Maron et al., 2013]; or
- Effect of Γ_{ii} on Stark lineshapes of high- n transitions [Alumot et al., 2017] (in preparation).

Plasma parameters inferred

Assuming the plasma is uniform, we obtain

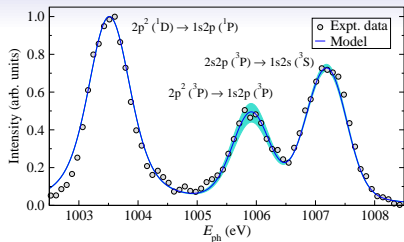
- Plasma radius r_{pl} – from the pinhole x-ray imaging;
- Electron density n_e – from the satellite ratios;
- Electron temperature T_e – from the time-dependent collisional-radiative (CR) model satisfying both the absolute PCD signal I_{PCD} and time-integrated continuum slope;
- T_i^{eff} – from the satellite Doppler broadening (the Stark width is negligible);

T_i is inferred from the data above, plus using either

- Detailed energy-balance analysis [Kroupp et al., 2011, Maron et al., 2013]; or
- Effect of Γ_{ii} on Stark lineshapes of high- n transitions [Alumot et al., 2017] (in preparation).

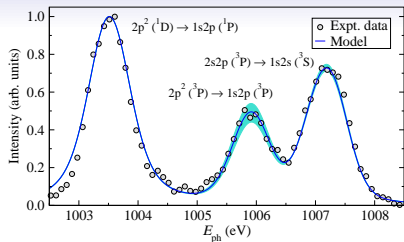
This modeling described all the data very well, within 1 – 2 std. dev.

Determination of n_e and T_i^{eff}

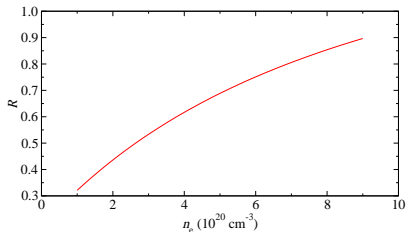


Widths and intensities of the Ne Ly- α satellites allow for determining T_i^{eff} and n_e , respectively. In this example, $T_i^{\text{eff}} = 1200 \text{ eV}$ and $n_e = (5 \pm 1) \times 10^{20} \text{ cm}^{-3}$.

Determination of n_e and T_i^{eff}



Widths and intensities of the Ne Ly- α satellites allow for determining T_i^{eff} and n_e , respectively. In this example, $T_i^{\text{eff}} = 1200$ eV and $n_e = (5 \pm 1) \times 10^{20} \text{ cm}^{-3}$.



$I_{2p^2(^3P) \rightarrow 1s2p(^3P)} / I_{2s2p(^3P) \rightarrow 1s2s(^3S)}$ intensity ratio R is sensitive to n_e but practically independent of T_e [Seely, 1979, Kroupp et al., 2007].

Determination of T_i during z-pinch stagnation

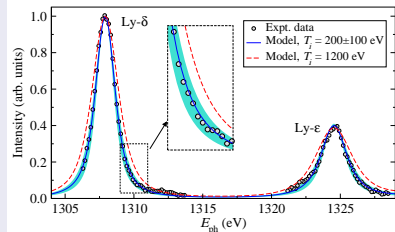
Two methods have been used:

1. Detailed energy-balance analysis

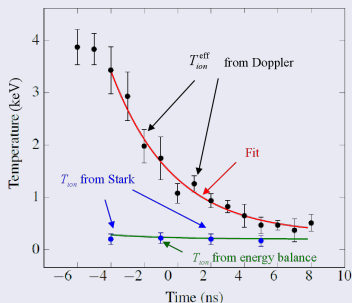
$$\frac{T_i - T_e}{\tau_{ie}} = \frac{dT_i^{\text{eff}}}{dt}$$

[Kroupp et al., 2011]

2. Effect of Γ_{ii} on Stark lineshapes



[Alumot et al., 2017] (in preparation)



Both methods give the same, consistent results.

Hypothesis: turbulent hydromotion

It was inferred that, at the stagnation phase,

- the ion kinetic energy at the stagnation phase is dominantly stored in non-thermal hydrodynamic motion;

Hypothesis: turbulent hydromotion

It was inferred that, at the stagnation phase,

- the ion kinetic energy at the stagnation phase is dominantly stored in non-thermal hydrodynamic motion;
- the plasma appeared largely uniform at spatial and temporal scales down to $\sim 100 \mu\text{m}$ and $\sim 1 \text{ ns}$, respectively;

Hypothesis: turbulent hydromotion

It was inferred that, at the stagnation phase,

- the ion kinetic energy at the stagnation phase is dominantly stored in non-thermal hydrodynamic motion;
- the plasma appeared largely uniform at spatial and temporal scales down to $\sim 100 \mu\text{m}$ and $\sim 1 \text{ ns}$, respectively;
- the Reynolds number is high ($\sim 10^5$);

Hypothesis: turbulent hydromotion

It was inferred that, at the stagnation phase,

- the ion kinetic energy at the stagnation phase is dominantly stored in non-thermal hydrodynamic motion;
- the plasma appeared largely uniform at spatial and temporal scales down to $\sim 100 \mu\text{m}$ and $\sim 1 \text{ ns}$, respectively;
- the Reynolds number is high ($\sim 10^5$);
- the flow is supersonic.

Hypothesis: turbulent hydromotion

It was inferred that, at the stagnation phase,

- the ion kinetic energy at the stagnation phase is dominantly stored in non-thermal hydrodynamic motion;
- the plasma appeared largely uniform at spatial and temporal scales down to $\sim 100 \mu\text{m}$ and $\sim 1 \text{ ns}$, respectively;
- the Reynolds number is high ($\sim 10^5$);
- the flow is supersonic.

Turbulence is an obvious candidate for such a significant small-scale hydrodynamic motion.

Hypothesis: turbulent hydromotion

It was inferred that, at the stagnation phase,

- the ion kinetic energy at the stagnation phase is dominantly stored in non-thermal hydrodynamic motion;
- the plasma appeared largely uniform at spatial and temporal scales down to $\sim 100 \mu\text{m}$ and $\sim 1 \text{ ns}$, respectively;
- the Reynolds number is high ($\sim 10^5$);
- the flow is supersonic.

Turbulence is an obvious candidate for such a significant small-scale hydrodynamic motion.

Were supersonic turbulence present, it would imply substantial nonuniformity in quantities such as the density. However, the previous analysis assumed a uniform plasma.

New analysis

The data need to be re-analyzed assuming a physically sound model of turbulence. [Kroupp et al., 2017]

Instead of $n_e = n_e^0 = \text{const}$, there is now a probability distribution function (PDF) $P(n_e)$ – actually, $P(t, z; n_e)$.

New analysis

The data need to be re-analyzed assuming a physically sound model of turbulence. [Kroupp et al., 2017]

Instead of $n_e = n_e^0 = \text{const}$, there is now a probability distribution function (PDF) $P(n_e)$ – actually, $P(t, z; n_e)$.

Let us switch to dimensionless quantity

$$\xi \equiv n_e/n_e^0; \int P(\xi) d\xi = 1.$$

The average density is

$$\langle n_e \rangle = n_e^0 \int \xi P(\xi) d\xi.$$

(note that $\langle n_e \rangle \neq n_e^0$).

Assuming the collisional-radiative equilibrium is established much faster than the hydromotion, the intensity of a spectral line (or continuum radiation) is [Stamm et al., 2017]

$$\langle I \rangle = \int \alpha(\vec{r}) d^3 r = \pi r_{\text{pl}}^2 \ell \int \alpha(\xi) P(\xi) d\xi,$$

where $\alpha \propto \xi^2$ is the local plasma emissivity, and r_{pl} and ℓ is the radius and length of the plasma segment, respectively.

Assuming the collisional-radiative equilibrium is established much faster than the hydromotion, the intensity of a spectral line (or continuum radiation) is [Stamm et al., 2017]

$$\langle I \rangle = \int \alpha(\vec{r}) d^3 r = \pi r_{\text{pl}}^2 \ell \int \alpha(\xi) P(\xi) d\xi,$$

where $\alpha \propto \xi^2$ is the local plasma emissivity, and r_{pl} and ℓ is the radius and length of the plasma segment, respectively.

In particular, the *absolutely calibrated* PCD signal is

$$I_{\text{PCD}} \propto \pi r_{\text{pl}}^2 \ell \int \xi^2 P(\xi) d\xi.$$

Assuming the collisional-radiative equilibrium is established much faster than the hydromotion, the intensity of a spectral line (or continuum radiation) is [Stamm et al., 2017]

$$\langle I \rangle = \int \alpha(\vec{r}) d^3 r = \pi r_{\text{pl}}^2 \ell \int \alpha(\xi) P(\xi) d\xi,$$

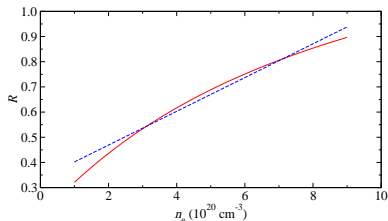
where $\alpha \propto \xi^2$ is the local plasma emissivity, and r_{pl} and ℓ is the radius and length of the plasma segment, respectively.

In particular, the *absolutely calibrated* PCD signal is

$$I_{\text{PCD}} \propto \pi r_{\text{pl}}^2 \ell \int \xi^2 P(\xi) d\xi.$$

$$\left(1 - \frac{\delta I_{\text{PCD}}}{I_{\text{PCD}}}\right) \left(\frac{r_{\text{pl}}^0}{r_{\text{max}}}\right)^2 \leq \int \xi^2 P(\xi) d\xi \leq \left(1 + \frac{\delta I_{\text{PCD}}}{I_{\text{PCD}}}\right) \left(\frac{r_{\text{pl}}^0}{r_{\text{min}}}\right)^2.$$

Density determination:

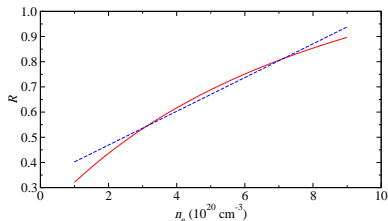


Use linearization

$R \approx R^0 + a_R(n_e/n_e^0 - 1)$, so

$$\langle R \rangle = R^0 + a_R \frac{\int (\xi - 1) \xi^2 P(\xi) d\xi}{\int \xi^2 P(\xi) d\xi}.$$

Density determination:



Use linearization

$R \approx R^0 + a_R(n_e/n_e^0 - 1)$, so

$$\langle R \rangle = R^0 + a_R \frac{\int (\xi - 1) \xi^2 P(\xi) d\xi}{\int \xi^2 P(\xi) d\xi}.$$

The measured quantity R_{expt} is known – **and should remain** – within its error bars, i.e., $\langle R \rangle = R_{\text{expt}} = R^0 \pm \delta R$. Therefore,

$$1 - \frac{\delta R}{a_R} \leq \frac{\int \xi^3 P(\xi) d\xi}{\int \xi^2 P(\xi) d\xi} \leq 1 + \frac{\delta R}{a_R}.$$

To summarize:

$$\left(1 - \frac{\delta I_{\text{PCD}}}{I_{\text{PCD}}}\right) \left(\frac{r_{\text{pl}}^0}{r_{\text{max}}}\right)^2 \leq \int \xi^2 P(\xi) d\xi \leq \left(1 + \frac{\delta I_{\text{PCD}}}{I_{\text{PCD}}}\right) \left(\frac{r_{\text{pl}}^0}{r_{\text{min}}}\right)^2 .$$

$$1 - \frac{\delta R}{a_R} \leq \frac{\int \xi^3 P(\xi) d\xi}{\int \xi^2 P(\xi) d\xi} \leq 1 + \frac{\delta R}{a_R} .$$

To summarize:

$$\left(1 - \frac{\delta I_{\text{PCD}}}{I_{\text{PCD}}}\right) \left(\frac{r_{\text{pl}}^0}{r_{\text{max}}}\right)^2 \leq \int \xi^2 P(\xi) d\xi \leq \left(1 + \frac{\delta I_{\text{PCD}}}{I_{\text{PCD}}}\right) \left(\frac{r_{\text{pl}}^0}{r_{\text{min}}}\right)^2 .$$

$$1 - \frac{\delta R}{a_R} \leq \frac{\int \xi^3 P(\xi) d\xi}{\int \xi^2 P(\xi) d\xi} \leq 1 + \frac{\delta R}{a_R} .$$

Once $P(\xi)$ is determined, the model plasma radius is corrected:

$$r_{\text{pl}} = r_{\text{pl}}^0 / \sqrt{\langle \xi^2 \rangle} .$$

Constraints on $P_V(\xi_V)$ and β

The last step is to use the volumetric density distribution:

$$\int P_V(\xi_V) d\xi_V = 1, \quad \int \xi_V P_V(\xi_V) d\xi_V = 1.$$

Introduce $\beta \equiv \xi/\xi_V = \langle n_e \rangle/n_e^0$; so $\langle \xi^k \rangle = \beta^k \langle \xi_V^k \rangle$.

Constraints on $P_V(\xi_V)$ and β

The last step is to use the volumetric density distribution:

$$\int P_V(\xi_V) d\xi_V = 1, \quad \int \xi_V P_V(\xi_V) d\xi_V = 1.$$

Introduce $\beta \equiv \xi/\xi_V = \langle n_e \rangle/n_e^0$; so $\langle \xi^k \rangle = \beta^k \langle \xi_V^k \rangle$.

Finally:

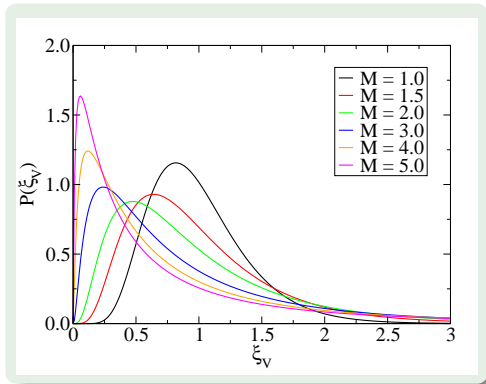
$$\sqrt{\frac{1 - \frac{\delta I_{\text{PCD}}}{I_{\text{PCD}}}}{\langle \xi_V^2 \rangle}} \frac{r_{\text{pl}}^0}{r_{\text{max}}} \leq \beta \leq \sqrt{\frac{1 + \frac{\delta I_{\text{PCD}}}{I_{\text{PCD}}}}{\langle \xi_V^2 \rangle}} \frac{r_{\text{pl}}^0}{r_{\text{min}}}$$

$$\left(1 - \frac{\delta R}{a_R}\right) \frac{\langle \xi_V^2 \rangle}{\langle \xi_V^3 \rangle} \leq \beta \leq \left(1 + \frac{\delta R}{a_R}\right) \frac{\langle \xi_V^2 \rangle}{\langle \xi_V^3 \rangle}$$

$$r_{\text{pl}} = r_{\text{pl}}^0 / (\beta \sqrt{\langle \xi_V^2 \rangle})$$

Volumetric PDF of [Hopkins, 2013]:

$$P_V(\xi_V) d\xi_V = \frac{I_1(2\sqrt{\lambda\omega(\xi_V)})}{\exp[\lambda + \omega(\xi_V)]} \sqrt{\frac{\lambda}{\theta^2\omega(\xi_V)}} \frac{d\xi_V}{\xi_V}$$



Here,

$$\lambda \equiv (1 + \theta)^{3/2} \ln(1 + M_c^2) / 2\theta^2$$

$$\omega(\xi_V) \equiv \lambda / (1 + \theta) - \ln(\xi_V) / \theta$$

$$\theta \approx 0.05M_c$$

Compressive Mach number

$$M_c = bM, \quad b \approx 0.4$$

I_1 – modified Bessel function
of the first kind

Constraints on $P_V(\xi_V)$ and β

The last step is to use the volumetric density distribution:

$$\int P_V(\xi_V) d\xi_V = 1, \quad \int \xi_V P_V(\xi_V) d\xi_V = 1.$$

Introduce $\beta \equiv \xi/\xi_V = \langle n_e \rangle/n_e^0$; so $\langle \xi^k \rangle = \beta^k \langle \xi_V^k \rangle$.

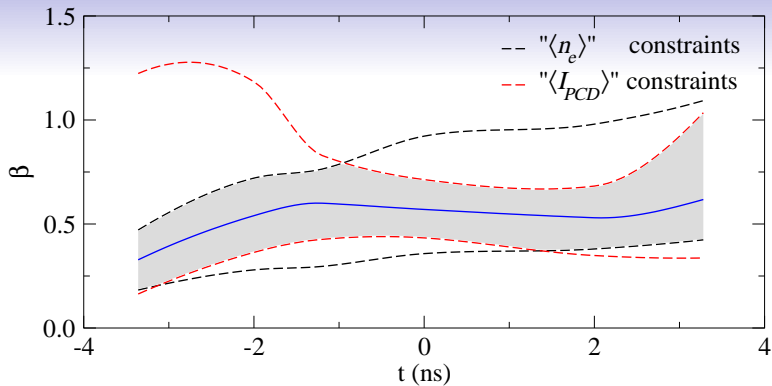
Finally:

$$\sqrt{\frac{1 - \frac{\delta I_{\text{PCD}}}{I_{\text{PCD}}}}{\langle \xi_V^2 \rangle}} \frac{r_{\text{pl}}^0}{r_{\text{max}}} \leq \beta \leq \sqrt{\frac{1 + \frac{\delta I_{\text{PCD}}}{I_{\text{PCD}}}}{\langle \xi_V^2 \rangle}} \frac{r_{\text{pl}}^0}{r_{\text{min}}}$$

$$\left(1 - \frac{\delta R}{a_R}\right) \frac{\langle \xi_V^2 \rangle}{\langle \xi_V^3 \rangle} \leq \beta \leq \left(1 + \frac{\delta R}{a_R}\right) \frac{\langle \xi_V^2 \rangle}{\langle \xi_V^3 \rangle}$$

$$r_{\text{pl}} = r_{\text{pl}}^0 / (\beta \sqrt{\langle \xi_V^2 \rangle})$$

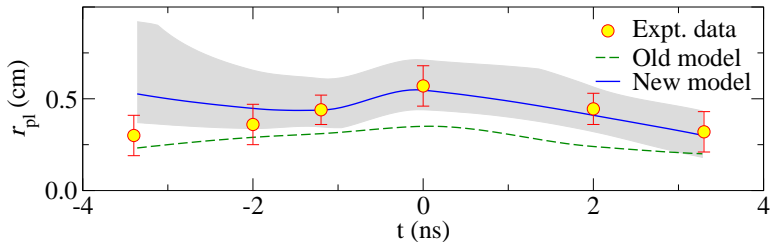
Results: model mean density and plasma radius



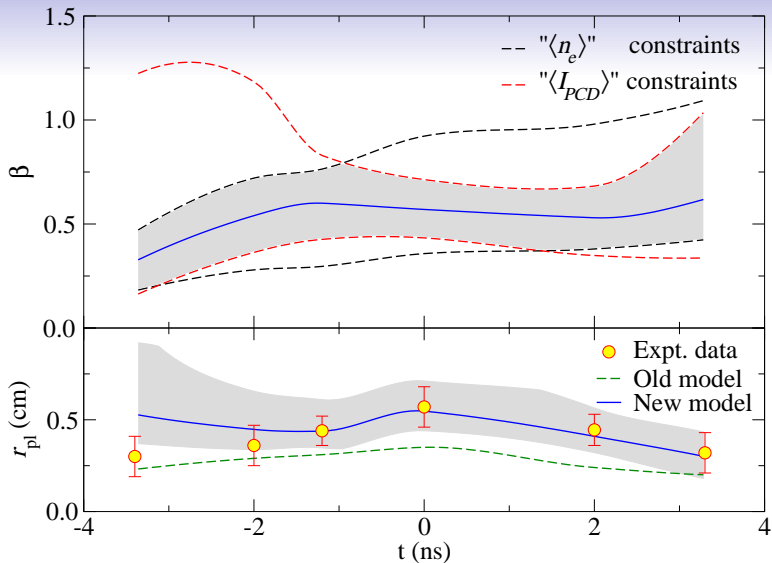
The mean plasma density is inferred to be lower by a factor ~ 2 .

Results: model mean density and plasma radius

The corrected plasma model radius fits the data better.



Results: model mean density and plasma radius



The other plasma parameters (T_e , T_i , and T_i^{eff}) remain unaffected.

Results in a wider scientific context

In addition to better understanding of z-pinch stagnation plasmas, a crucial question arises:

Is the supersonic turbulent hydromotion generated and carried along during the implosion phase?

Results in a wider scientific context

In addition to better understanding of z-pinch stagnation plasmas, a crucial question arises:

Is the supersonic turbulent hydromotion generated and carried along during the implosion phase?

If yes (and we have preliminary results confirming it), then z-pinchs represent a test bed for:

- a recently proposed novel fast ignition scheme [Davidovits and Fisch, 2016] for inertial confinement;
- astrophysical phenomena, such as molecular cloud dynamics, star formation efficiency, the core mass/stellar initial mass function, and more.

Conclusions

- Inferred $T_i \ll T_i^{\text{eff}}$ at z-pinch stagnation, with $\text{Re} \sim 10^5$ and observing no large-scale plasma non-uniformities, strongly hints at turbulence; supersonic one ($M \sim 1 - 2$).

Conclusions

- Inferred $T_i \ll T_i^{\text{eff}}$ at z-pinch stagnation, with $\text{Re} \sim 10^5$ and observing no large-scale plasma non-uniformities, strongly hints at turbulence; supersonic one ($M \sim 1 - 2$).
- Analysis with the uniform-plasma assumption lifted shows that the picture of a preponderance of turbulent energy remains intact.

Conclusions

- Inferred $T_i \ll T_i^{\text{eff}}$ at z-pinch stagnation, with $\text{Re} \sim 10^5$ and observing no large-scale plasma non-uniformities, strongly hints at turbulence; supersonic one ($M \sim 1 - 2$).
- Analysis with the uniform-plasma assumption lifted shows that the picture of a preponderance of turbulent energy remains intact.
- As a result, the mean plasma density is inferred to be lower by a factor ~ 2 .

Conclusions

- Inferred $T_i \ll T_i^{\text{eff}}$ at z-pinch stagnation, with $\text{Re} \sim 10^5$ and observing no large-scale plasma non-uniformities, strongly hints at turbulence; supersonic one ($M \sim 1 - 2$).
- Analysis with the uniform-plasma assumption lifted shows that the picture of a preponderance of turbulent energy remains intact.
- As a result, the mean plasma density is inferred to be lower by a factor ~ 2 .
- This turbulent-plasma model is not only consistent with the observations, it improves the agreement with them (r_{pl}).

- Inferred $T_i \ll T_i^{\text{eff}}$ at z-pinch stagnation, with $\text{Re} \sim 10^5$ and observing no large-scale plasma non-uniformities, strongly hints at turbulence; supersonic one ($M \sim 1 - 2$).
- Analysis with the uniform-plasma assumption lifted shows that the picture of a preponderance of turbulent energy remains intact.
- As a result, the mean plasma density is inferred to be lower by a factor ~ 2 .
- This turbulent-plasma model is not only consistent with the observations, it improves the agreement with them (r_{pl}).
- Beyond aiding our understanding of z-pinches, we hope this study can provide fertile ground for dealing with related problems of astrophysical interest.

Thank you!

Bibliography I



Alumot, D., Kroupp, E., Stambulchik, E., Maron, Y., and Fisher, A. (2017).
Determination of ion temperature in high-energy-density plasmas using the Stark
effect.
In preparation.



Davidovits, S. and Fisch, N. J. (2016).
Phys. Rev. Lett., 116(10):105004.



Foord, M. E., Maron, Y., Davara, G., Gregorian, L., and Fisher, A. (1994).
Phys. Rev. Lett., 72:3827–3830.



Hopkins, P. F. (2013).
Mon. Not. R. Astron. Soc., 430(3):1880.



Kroupp, E., D. Osin, Starobinets, A., Fisher, V., Bernshtam, V., Maron, Y., Uschmann,
I., Förster, E., Fisher, A., and Deeney, C. (2007).
Phys. Rev. Lett., 98:115001.



Kroupp, E., Osin, D., Starobinets, A., Fisher, V., Bernshtam, V., Weingarten, L.,
Maron, Y., Uschmann, I., Förster, E., Fisher, A., Cuneo, M. E., Deeney, C., and
Giuliani, J. L. (2011).
Phys. Rev. Lett., 107:105001.

Bibliography II



Kroupp, E., Stambulchik, E., Starobinets, A., Osin, D., Fisher, V. I., Alumot, D., Maron, Y., Davidovits, S., Fisch, N. J., and Fruchtmann, A. (2017).

arXiv:1705.03114 [physics].

Submitted to *Phys. Rev. Lett.*



Maron, Y., Starobinets, A., Fisher, V. I., Kroupp, E., Osin, D., Fisher, A., Deeney, C., Coverdale, C., Lepell, P. D., Yu, E., Jennings, C., Cuneo, M. E., Herrmann, M. C., Porter, J. L., Velikovich, A., Mehlhorn, T., and Apruzese, J. P. (2013).

Phys. Rev. Lett., 111:035001.



Osin, D., Kroupp, E., Starobinets, A., Rosenzweig, G., Alumot, D., Maron, Y., Fisher, A., Yu, E., Giuliani, J. L., and Deeney, C. (2011).

Plasma Science, IEEE Transactions on, 39(11):2392–2393.



Osterbrock, D. E., Miller, J. S., and Weedman, D. W. (1966).

Astrophys. J., 145:697–707.



Seely, J. F. (1979).

Phys. Rev. Lett., 42:1606–1609.



Stamm, R., Hannachi, I., Meireni, M., Capes, H., Godbert-Mouret, L., Koubiti, M., Rosato, J., Marandet, Y., Dimitrijević, M., and Simić, Z. (2017).

Eur. Phys. J. D, 71(3):68.



You, S., Yun, G. S., and Bellan, P. M. (2005).
Phys. Rev. Lett., 95(4):045002.



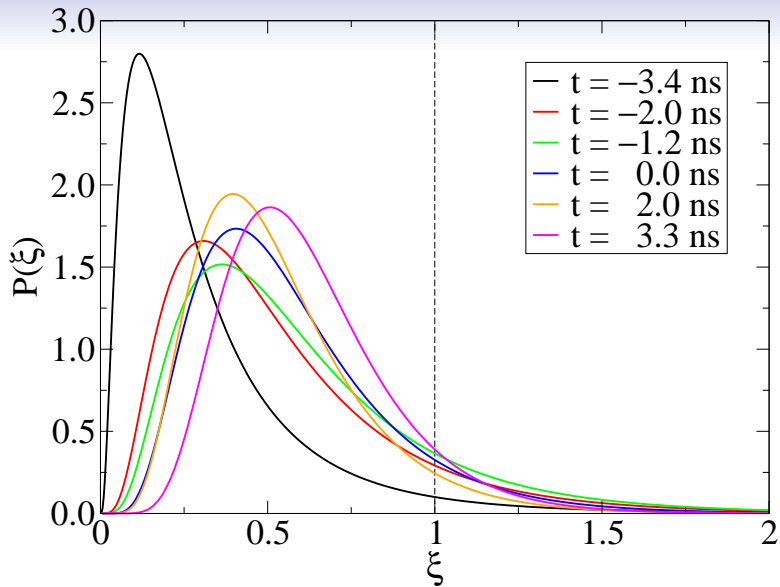
Zeldovich, Ya. B. and Raizer, Yu. (1967).
Physics of shock waves and high-temperature hydrodynamic phenomena.
Academic Press, New York.

Data summary

The experimental data [Kroupp et al., 2011] relevant for the analysis presented; the plasma parameters assumed for $(r_{\text{pl}}^0, n_e^0, T_e)$ and inferred from (T_i, M, Re) the *uniform*-plasma modeling; the calculated isothermal turbulence parameters, volumetric density factor β and respectively corrected plasma electron density and radius. Units are as follows: all radii are in mm, all temperatures are in eV, and densities are in 10^{20} cm^{-3} .

t (ns)	Experimental data					Uniform plasma						Isothermal turbulence						
	δR	I_{PCD} (GW)	r_{min}	r_{max}	T_i^{eff}	r_{pl}^0	n_e^0	T_e	T_i	M	Re	θ	$\sigma_{s,V}^2$	$\langle \xi_V^2 \rangle$	$\langle \xi_V^3 \rangle$	β	n_e^{turb}	$r_{\text{pl}}^{\text{turb}}$
-3.4	0.15	0.35 ± 0.3	0.19	0.41	3000	0.23	6.0	120	250	2.4	8.1×10^4	0.048	0.70	1.84	5.77	0.32	1.9	0.53
-2.0	0.15	2.0 ± 1.0	0.25	0.47	2100	0.29	6.0	175	230	1.7	6.9×10^4	0.034	0.40	1.44	2.86	0.54	3.2	0.45
-1.2	0.15	3.8 ± 1.1	0.36	0.52	1800	0.31	6.0	190	210	1.6	7.7×10^4	0.032	0.36	1.39	2.60	0.60	3.6	0.44
0.0	0.15	6.5 ± 0.7	0.46	0.68	1300	0.35	6.0	185	200	1.3	8.9×10^4	0.026	0.25	1.26	1.96	0.57	3.4	0.55
2.0	0.15	3.6 ± 1.0	0.36	0.53	900	0.24	6.0	155	180	1.2	7.4×10^4	0.024	0.21	1.22	1.80	0.53	3.2	0.41
3.3	0.15	2.3 ± 0.9	0.21	0.43	720	0.20	6.0	140	180	1.0	5.1×10^4	0.020	0.15	1.16	1.53	0.62	3.7	0.30

Results: turbulent density PDF's



Is turbulence in this stagnating plasma isothermal?

Compare v_{flow} to a thermal conduction velocity (following [Zeldovich and Raizer, 1967]),

$$v_{\text{cond}} = \frac{L_h}{\tau_{\text{cond}}} \approx 4 \times 10^{21} \frac{\zeta(\langle Z_i \rangle)}{(\langle Z_i \rangle + 1) \lambda_{ei} n_e L_h} T^{5/2},$$

where L_h is a length scale ($L_h \sim r_{\text{pl}}$), λ_{ei} is the Coulomb logarithm, and $\zeta(8.5) \approx 2.7$; T is in units of eV, n_e in cm^{-3} , and L_h in cm.

When $v_{\text{cond}}/v_{\text{flow}} \gg 1$, isothermality is expected.

$v_{\text{cond}}/v_{\text{flow}} \sim 2$ for $L_h \sim r_{\text{pl}}$ at $t = -3.4$ ns, and ~ 6 for later times.

An accurate determination of the degree of isothermality would require detailed simulations. The inferred T_e will also need to be reconsidered, since the emissivity depends on T_e strongly.

Interestingly, in Sandia Z experiments, where T_e and $\langle Z_i \rangle$ reach higher values, $v_{\text{cond}}/v_{\text{flow}} \gg 1$, thus the assumption of turbulence isothermality should be fully justified.